RESEARCH ARTICLE | SEPTEMBER 06 2023

Effects of superhydrophobicity on VIV control of a circular cylinder

Special Collection: Superhydrophobic Surfaces

Fuwang Zhao ; Lingwei Zeng ; Zhaokun Wang ; Yang Liu ; Li Li ; Hui Tang

Appl. Phys. Lett. 123, 101603 (2023)
https://doi.org/10.1063/5.0159879

Applied Physics Letters ARTICLE pubs.aip.org/aip/apl

Effects of superhydrophobicity on VIV control of a circular cylinder

Cite as: Appl. Phys. Lett. **123**, 101603 (2023); doi: 10.1063/5.0159879
Submitted: 28 May 2023 · Accepted: 23 August 2023 ·
Published Online: 6 September 2023

Fuwang Zhao,[1,2,3] Lingwei Zeng,[1,2] Zhaokun Wang,[1,2,3] Yang Liu,[1] Li Li,[3] and Hui Tang[1,2,a)]

AFFILIATIONS

[1]Department of Mechanical Engineering, The Hong Kong Polytechnic University, Kowloon, Hong Kong, China
[2]The Hong Kong Polytechnic University Shenzhen Research Institute, Shenzhen, Guangdong 518057, China
[3]School of Fashion and Textiles, The Hong Kong Polytechnic University, Kowloon, Hong Kong, China

Note: This paper is part of the APL Special Collection on Superhydrophobic Surfaces.
[a)]**Author to whom correspondence should be addressed:** h.tang@polyu.edu.hk

ABSTRACT

We conducted an experimental study on the vortex-induced vibration (VIV) dynamics of cylinders featuring a specific superhydrophobic band. The superhydrophobic band refers to the pattern where the cylinder's surface is featured with equispaced bands of normal surface and superhydrophobic coating in an alternate manner. The experiments were conducted over a range of reduced velocities from $U_r = 3$ to 11, corresponding to Reynolds numbers between 1500 and 5900. To capture the near-field wake of the cylinders, a time-resolved particle image velocimetry (TR-PIV) system was employed, while the hydrodynamic forces were acquired using a six-component load cell. We found that the fully coated cylinder consistently displays the smallest amplitude of oscillation in the VIV initial branch, achieving a maximum reduction of approximately 38.9% at $U_r = 5.0$. Upon applying a superhydrophobic coated band, the patterned cylinder experiences a substantial enhancement in VIV amplitude (about 22.5% at $U_r = 5.0$) compared to the normal cylinder. On the other hand, in the VIV lower branch, the patterned cylinder effectively suppresses oscillation, whereas the fully coated cylinder exhibits slightly larger oscillation amplitudes than the normal cylinder. This finding agrees well with the trend of lift forces. The analysis of phase-averaged flow structures suggests that this difference can be attributed to the delayed vortex shedding from the superhydrophobic surface and the emergence of three-dimensional vortex structures created by the superhydrophobic band.

Flow-induced vibration (FIV) poses significant challenges in various structures, including cooling towers, high-rise buildings, and heat exchangers, due to its potential for fatigue, reduced lifespan, and catastrophic failures. To tackle these challenges, researchers have developed various methods to manipulate the dynamic response of bluff bodies, including active control techniques like rotation, jets, and plasma actuators, and passive control approaches, such as surface modification and the attachment of small rods or fin.[1–8] For a comprehensive exploration of passive control methods, we recommend consulting the most recent review papers.[9–13] Inspired by the water-repellent characteristics of lotus leaves, superhydrophobic surfaces have emerged as a viable mean for altering surface properties.[14] Since the surface properties can significantly influence the surface flow, some studies have been conducted to explore the effectiveness of hydrophobic surfaces in force reduction and vortex-induced vibration (VIV) suppression for cylinders.[15–24]

For fixed cylinders, You and Moin[15] conducted numerical investigations on the effects of hydrophobic surfaces by alternating slip and no-slip bands. They observed reductions in the drag and fluctuation lift, with the maximum reduction reaching 8.0% and 21.1%, respectively. Muralidhar *et al.*[18] further experimentally examined the impact of partial-slip conditions on flow past superhydrophobic circular cylinders. They found that superhydrophobic bands extended recirculation length and delayed vortex shedding onset. Kim *et al.*[21] confirmed the above observations. Their results indicated that the local hydrophobic coatings showed the most effective hydrodynamic control when applied near the cylinder's separation point. Recently, Sooraj *et al.*[24] also observed a maximum drag reduction of 15% at the Reynolds number $Re = \rho U_\infty D/\mu = 860$, where ρ, U_∞, D, and μ are the water density, incoming velocity, diameter, and dynamic viscosity of water, respectively. These studies collectively highlighted the potential of using hydrophobic surfaces in force suppression of fixed cylinders. However, till now rare literature focused on the effects of the superhydrophobic surfaces on elastically supported cylinders. However, only Daniello *et al.*[19] experimentally investigated the influence of superhydrophobicity of a VIV circular cylinder at $1300 \leq Re \leq 2300$. They

found that superhydrophobicity could diminish lift fluctuation and oscillating amplitude by up to 15% without affecting drag or natural frequency. Their PIV measurements indicated that superhydrophobicity increased the length and width of the vortex formation length as well as the intensity of shedding vortices, thus decreasing the VIV amplitude.

As indicated in the previous studies, the superhydrophobic surface can be regarded as a slip wall, resulting in an elongated recirculation zone behind the cylinder. Consequently, when fully coated with a superhydrophobic layer, a cylinder exhibits reduced vibration-induced vibration (VIV) in comparison with an uncoated cylinder. On the other hand, our recent studies indicated that modifying the cylinder's surface with a wavy pattern also contributes to VIV mitigation, especially when the spanwise wavelength is around $1.8D$.[7] This wavy cylinder's control mechanism can be elucidated by reducing the spanwise stability of vortices shed from a three-dimensional cylinder. This alteration effectively breaks down large, strong vortices into smaller, discrete vortices, thereby enhancing the dissipation of wake energy. Thus, in the present study, our objective is to explore the synergy of these two control mechanisms on VIV control by applying alternating superhydrophobic bands on the cylinder's surface.

Three aluminum circular cylinders with diameter $D = 22$ mm and length $L = 440$ mm were manufactured for the experiment, including a normal cylinder (without coating, $\lambda_z/D = 0$), cylinders with a superhydrophobic band at $\lambda_z/D = 1.8$, and a fully coated cylinder ($\lambda_z = \infty$), as shown in Figs. 1(a) and 1(b), where λ_z denotes the wavelength of the band. The coating process for the tested cylinders is as follows: first, Glaco[25] was uniformly sprayed onto the cylinders. Second, the cylinders were dried in an oven at 100 °C for a duration of 1 h. Third, steps 1 and 2 were repeated two additional times. The contact angles of the normal and superhydrophobic surfaces were measured using the tangent method,[22,25] as shown in Figs. 1(c) and 1(d). The advancing and receding contact angles for the superhydrophobic painted surface were determined as $\theta_a = 173° \pm 2°$ and $\theta_r = 169° \pm 2°$, respectively. These measurements align reasonably well with those reported by previous studies.[21,24,25] The contact angle of the normal surface was approximately $81° \pm 2°$.

The dynamic response measurement was conducted in a closed-loop water channel with flow speed ranging from 0.05 to 4.00 m/s. Figure 1(e) illustrates the test rig, where a cylinder is vertically placed at the center of the test section. This results in a blockage ratio of 7.3%, slightly surpassing the critical value of 5%, as advised by Holmes.[26] However, Lei *et al.*[27] and Lei and Sun[28] indicated that the experimental results were still very close to the theoretical predictions even when the blockage ratio reached 13.0%. This suggests that our experimental data remained compelling without involving any correction. The combined mass of the cylinder and its supporting shaft was approximately $m = 9.0$ kg, corresponding to a mass ratio of $m^* = 4m/\pi\rho D^2 L \approx 52$, where ρ denotes the water density. Through free decay tests, the system's structural damping was determined as $\zeta = 1.35 \times 10^{-3}$, resulting in $m^*\zeta = 0.07$. Due to such a large mass ratio, the effect of added mass is marginal. Thus, the difference between the natural frequency of cylinder in air and water is less than 1.7%, i.e., $f_N = f_{N,\text{water}} \approx f_{N,\text{air}} = 1.1$ Hz. During the experiments, the incoming flow velocity varies from 0.07 to 0.27 m/s, corresponding to a reduced velocity $U_r = U_\infty/f_N D = 3 \sim 11$ ($1500 < Re < 5900$). The upper end of the cylinder is connected with a load cell (ATI Mini-40) to measure the force. We capture the force signals using an analog-to-digital (A/D) converter (NI 9220) with a sampling rate of 2 kHz. To obtain the hydrodynamic force experienced by the cylinder, the inertial force should be subtracted from the measured force. To capture the cylinder's motions and its near wake synchronously, a high-speed camera (Photron Mini UX100) is employed from the side, which takes images through a 45°-inclined mirror placed underneath the water tunnel [Fig. 1(e)]. To minimize the experimental uncertainty, we performed four independent runs, with each run lasting over 180 s.

Figure 2(a) presents the VIV amplitude y^* as a function of reduced velocity U_r ($=U_\infty/f_N D$) for various selected cylinders. It is evident that all tested cylinders oscillation VIV at a similarly reduced velocity $U_r = 3.9$. Their VIV responses can be further divided into two branches: an initial branch characterized by a sharp increase in oscillation amplitude and a lower branch where the amplitude gradually decreases from its peak values to zero. This behavior is in line with previously reported findings with comparable $m^*\zeta$ values.[29–32] In the initial branch, the fully coated cylinder consistently exhibits the smallest y^* among all cases, with a maximum reduction of approximately

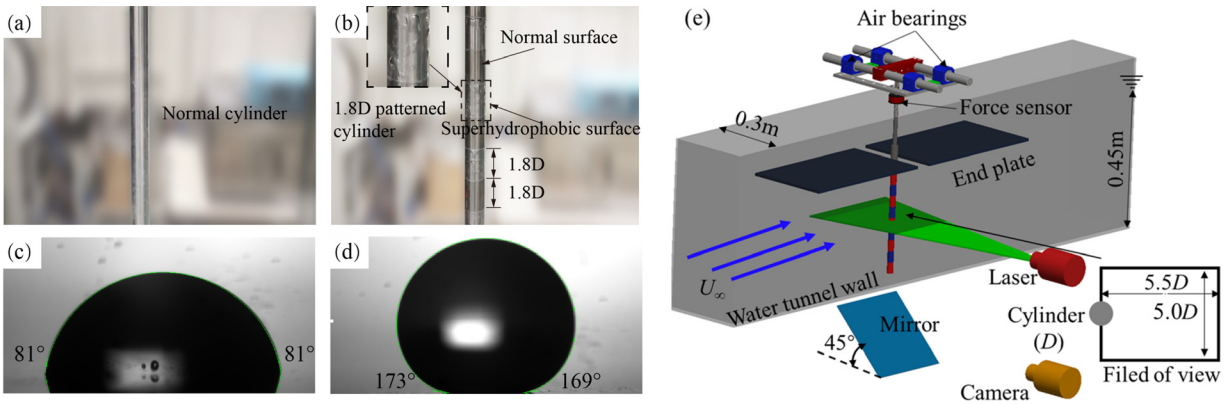

FIG. 1. Schematics of (a) a normal cylinder without any coating; (b) a patterned cylinder with alternating superhydrophobicity bands, i.e., its surface is featured with equispaced bands of normal surface and superhydrophobic coating in alternate manner; (c) and (d) contact-angles for the normal and patterned cylinder, respectively; and (e) schematic of the test rig and TR-PIV system used in a water channel. The close-up view on the top left corner of Fig. 1(b) is to indicate the bubbles (air interface) on the superhydrophobic surface of cylinder, which can be regarded as a partial slip boundary condition.

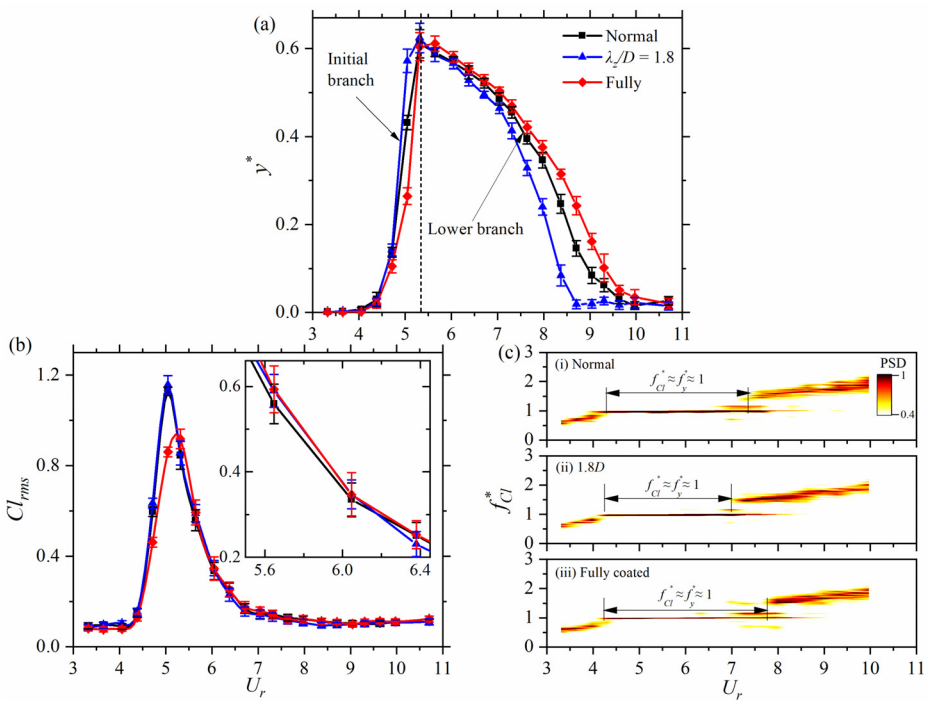

FIG. 2. (a) The oscillation amplitude y^*, (b) the *rms* lift coefficient Cl_{rms}, and (c) the dimensionless frequency of the lift force ($f_{Cl}^* = f_{Cl}/f_N$) of the selected cases vs reduced velocity U_r.

38.9% at $U_r = 5.0$. This observation confirms the findings of Daniello *et al.*[19] who attributed this phenomenon to the ability of the superhydrophobic surface to postpone the onset of vortex shedding, thus reducing the lift fluctuation and oscillation amplitude. When the superhydrophobic coated band is applied, the patterned cylinder experiences a significant enhancement in y^* (around 22.5% at $U_r = 5.0$) compared to the normal cylinder. In the lower branch, it is clearly found that the patterned cylinder exhibits a considerably smaller y^* compared to the normal cylinder. Conversely, the fully coated cylinder shows a slightly larger y^* than the normal cylinder. These observations indicate that the VIV amplitude curve for the patterned cylinder shifts toward lower U_r values, whereas the fully coated cylinder experiences a shift toward higher U_r values.

Lift fluctuation is a significant driving factor of fluid-induced vibration. Figure 2(b) shows the relationship between the root mean square value of lift coefficient (Cl_{rms}) and the reduced velocity (U_r). In the absence of oscillation, Cl_{rms} remains consistently low for all cases, around 0.1, where the fully coated cylinder consistently exhibits the lowest value *of* $Cl_{rms} \approx 0.08$. However, with the onset of oscillation, Cl_{rms} of all the cases sharply increases, reaching a peak value. Especially, both the normal cylinder and the patterned cylinder exhibit their peak Cl_{rms} values ($Cl_{rms} = 1.12$ and $Cl_{rms} = 1.16$, respectively) at $U_r = 5.0$. However, the fully patterned cylinder experiences a minimum peak value of $Cl_{rms} = 0.91$ at a slightly larger $U_r = 5.3$. As the freestream velocity continues to increase, the oscillation response of various cylinders stepped into the lower branch where Cl_{rms} decreases sharply until $U_r = 7.0$. After that, it gradually decreases further from $Cl_{rms} = 0.12$. At the start of this branch, the patterned cylinder consistently displays slightly lower Cl_{rms} values, while slightly higher Cl_{rms} values are observed for the fully patterned cylinder. Until $U_r = 7.0$, the difference among these selected cases is almost invisible. Overall, the general trend of Cl_{rms} closely follows the variations of y^*.

Due to the large mass ratio of our system ($m^* = 52$), the displacement oscillation frequency response remains close to $f_y^* = f_y/f_N \approx 1.0$ for all tested cases across the entire lock-in regime. This observation aligns with the previous studies.[5,33] Figure 2(c) further displays the normalized frequency (f_{cl}^*) of the lift force plotted against the reduced velocity (U_r) for the selected cases. It is evident that the patterned cylinder exhibits the narrowest lock-in range ($f_y^* \approx f_{cl}^* \approx 1$) among all the tested cases. It suggests that the lift and vibration of the patterned cylinder desynchronize with each other earlier than the other cases, which may be one reason for the least oscillation amplitudes observed in its lower branch. Conversely, the fully coated cylinder demonstrates a slightly wider lock-in range, leading to the largest oscillation amplitude in the lower branch.

Following the assumption used in Bearman[34] and Khalak and Williamson,[33] the transversal oscillation displacement $y(t)$ and the lift force $F(t)$ can be seen as a harmonic response of linear oscillator; hence,

$$F(t) = F_0 \sin(2\pi f t + \phi), \tag{1}$$

$$y(t) = y_0 \sin(2\pi f t), \tag{2}$$

where F_0 and y_0 are the amplitude of the lift force and transversal oscillation displacement, respectively; f is to describe the vibration and lift frequency; and ϕ is the phase difference between hydrodynamic force and oscillation displacement. To maintain the energy for VIV, the energy transferring from the flow to the elastic-supported cylinder can be expressed as

$$E = \int_0^{1/f} F(t)\dot{y}(t)dt = \pi F_0 y_0 \sin\phi. \tag{3}$$

The normalized form of the energy transferred from the wake is given as

$$E^* = \pi y_0 Cl_0 \sin\phi, \tag{4}$$

where Cl_0 is the amplitude of the lift coefficient. According to Eq. (4), it can be seen that the oscillation response does not directly depend on the lift force, but the lift force in phase with the body velocity, i.e., $Cl_0 \sin\phi$, which is usually seen as a "negative fluid-dynamic damping" induced by the flow structures.[31] To better understand the dynamic response of various cylinders, we plotted the phase difference between lift force and oscillation displacement and the energy transferred from flow structure E with a function of the reduced velocity U_r for them, respectively. Here, the value of ϕ is determined as $\phi = \arccos R(Cl, y)$, where $R(Cl, y)$ represents the correlation coefficient between the lift force Cl and the oscillation displacement y.

As shown in Fig. 3(a), at the onset of VIV ($U_r \approx 5.1$), ϕ undergoes a sudden transition from approximately 0° to around 170°, indicating the occurrence of lock-in phenomena. Subsequently, as the flow velocity enters the lower branch ($5.3 < U_r \leq 10.1$), ϕ gradually decreases to around 90°. In the initial branch, compared with the normal cylinder, the fully coated cylinder exhibits lower ϕ values, while the patterned cylinder shows slightly higher ϕ values. The opposite sceneries are observed in the first half of the lower branch, i.e., $5.3 < U_r \leq 7.5$. With the velocity further increasing, their differences in ϕ become marginal. Regarding the energy transferred from flow E^*, as illustrated in Fig. 3(b), the patterned cylinder consistently demonstrates the most pronounced E^*, yielding the largest vibration amplitude in the initial branch. In contrast, the fully coated cylinder exhibits the least E^*, reflecting oscillation suppression. In the lower branch, the patterned cylinder manifests the lowest E^*, corresponding to the least oscillation amplitude. Conversely, the fully coated cylinder enables enhanced energy transfer from the flow to the elastically supported structure, resulting in the largest oscillation amplitude among all the selected cases.

In order to examine the near wake of the cylinders, particle image velocimetry (PIV) measurements were performed in the mid horizontal plane for both the normal and fully coated cylinders. For the patterned cylinder, PIV measurements were conducted in three planes: the normal, the fully coated, and the interface between them. Two typical values of reduced velocity, namely, $U_r = 5.0$ and 8.4, were chosen because they showed substantial differences in VIV amplitude in the initial and lower branches, respectively.

Figure 4 presents a sequence of phase-averaged vorticity fields over half a cycle at $U_r = 5.0$. It is evident that the cylinders shed alternating single positive and negative vortices, resulting in the classical 2S vortex mode downstream of the cylinder [Fig. 4(a)]. This finding aligns with the studies conducted by Wang *et al.*[35] and Williamson and Govardhan.[36] For the fully coated cylinder and patterned cylinder, the 2S vortex mode can still be observed, as depicted in Figs. 4(b)–4(e). However, some differences exist between these two cases. Notably, as indicated in Fig. 4(b), the strength of the positive and negative vortices in the fully coated cylinder is weaker compared to the normal cylinder. Additionally, the vortices in the fully coated cylinder exhibit delayed development. These observations suggest that the presence of superhydrophobic surfaces suppresses and delays vortex formation on the fully coated cylinder. This phenomenon corroborates the findings reported by Legendre *et al.*[16] and Sooraj *et al.*[24] on fixed cylinders. In addition, the distance between the center of the negative and positive vortex, which indicates the VIV amplitude, exhibits a reduction in the fully coated cylinder relative to that of the normal cylinder at various instances. Regarding the patterned cylinder, the wake in the coated cross section also experiences delayed development compared to the normal cross section [Figs. 4(c) and 4(e)]. The interface cross section between these two sections exhibits an intermediate wake distribution compared to the coated and normal cross sections [Fig. 4(d)]. These observations indicate the three-dimensionality of the flow structures associated with the 1.8D patterned cylinder.

Figure 5 shows the phase-averaged vorticity profiles of the normal, fully coated, and patterned cylinders at $U_r = 8.4$. It can be found that all the cases generate a pair of positive and negative vortices during each half cycle, leading to the emergence of the well-established 2P vortex shedding mode. Williamson and Govardhan[36] noted a comparable wake distribution in the lower branch when investigating the dynamic response of an elastically supported circular cylinder. Furthermore, in comparison with the normal cylinder, the fully coated cylinder exhibits an increased distance between the positive and negative vortices, indicating a notable amplification of vibration amplitude [see Figs. 5(a) and 5(b)]. This finding is consistent with the observed similarity between the oscillation and lift forces, as depicted in Fig. 2. Regarding the patterned cylinder, distinct differences become apparent when comparing the three analyzed cross sections [see Figs. 5(c)–5(e)]. This implies the presence of intricate three-dimensional flow patterns, akin to those observed in Figs. 4(c)–4(e). Furthermore, when compared to standard or completely coated cylinders, the gap in the cross-stream direction between the positive and negative vortices is reduced within this particular patterned arrangement. This suggests a suppression of oscillations for the patterned cylinder.

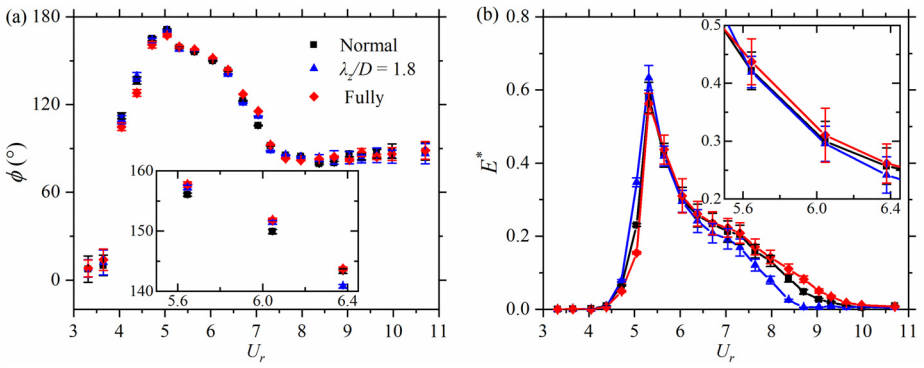

FIG. 3. (a) The phase difference between hydrodynamic force and oscillation displacement ϕ, (b) energy transferred from flow to structure over one cycle E^* of the selected cases vs reduced velocity U_r.

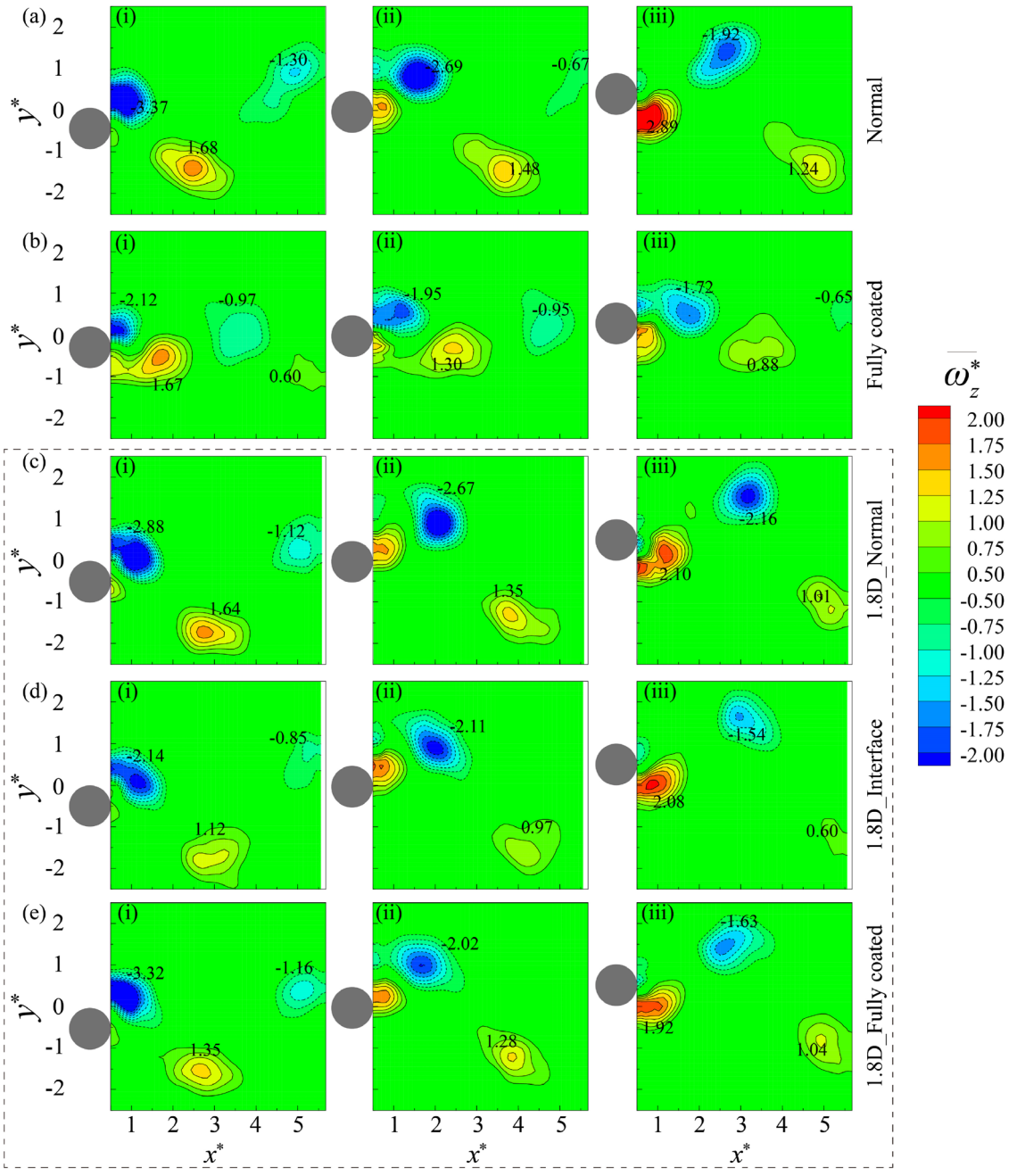

FIG. 4. Phase-averaged vortex patterns around selected cylinders (a) normal (b) fully coated (c)–(e) 1.8*D* patterned cylinder ($\lambda_z/D = 1.8$) in the normal, interface and fully coated part, respectively, at $U_r = 5.0$ where (i)–(iii) correspond to the location of the oscillating cylinder at $y^* = -y_0$, 0, and y_0.

In summary, the effects of the superhydrophobicity on the VIV amplitude, hydrodynamic forces, and wake structures are experimentally investigated with three typical cylinders, including a normal cylinder (without coating, $\lambda_z/D = 0$), a cylinder with the superhydrophobic bands at $\lambda_z/D = 1.8$, and a fully coated cylinder ($\lambda_z = \infty$). The present investigation leads to the following conclusions.

(1) All tested cylinders exhibit oscillations at a similarly reduced velocity ($U_r = 3.9$). Their amplitude responses can be further divided into two branches: an initial branch characterized by a sharp increase in oscillation amplitude and a lower branch where the amplitude gradually decreases from its peak values to zero.

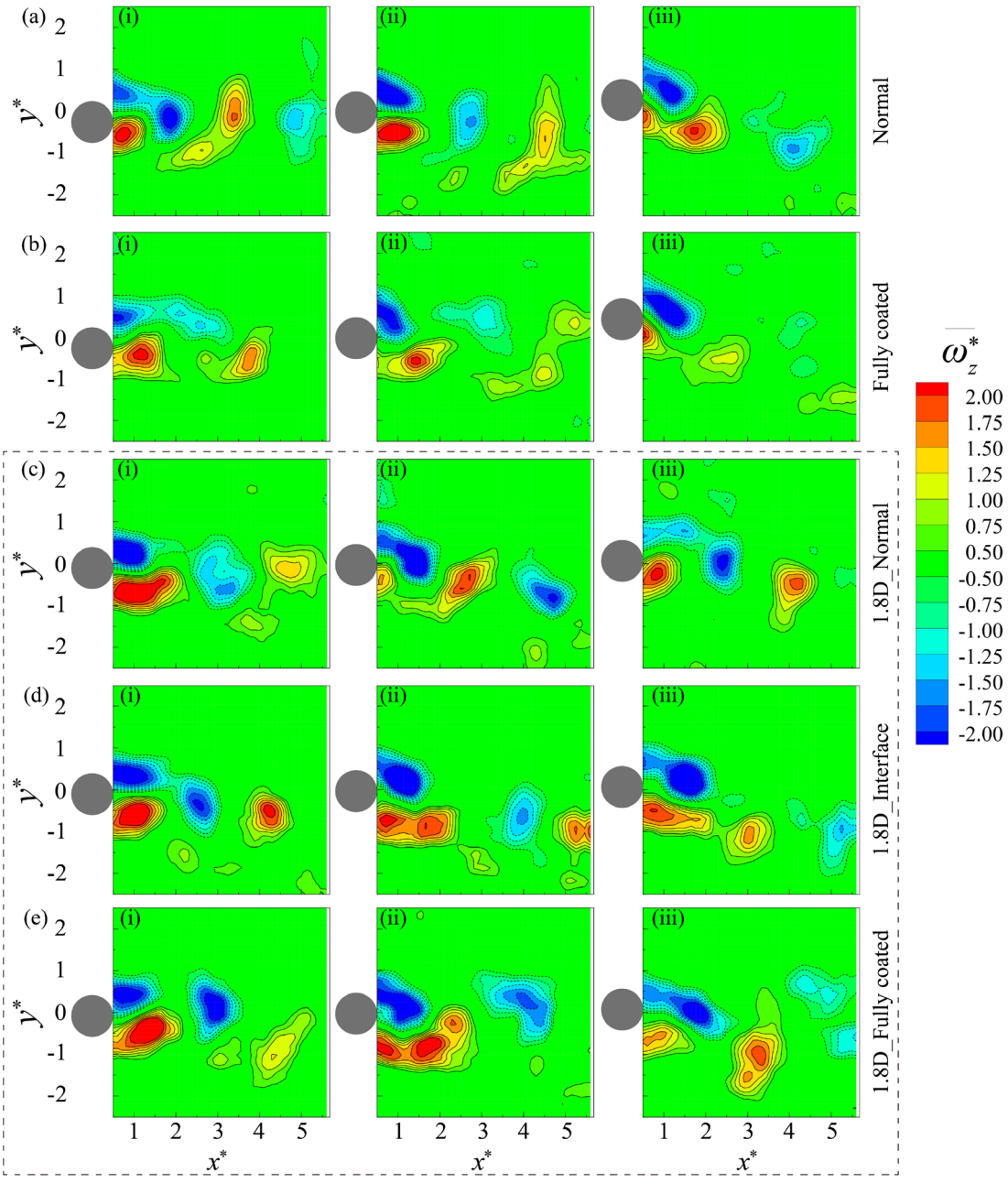

FIG. 5. Phase-averaged vortex patterns around selected cylinders (a) normal (b) fully coated (c)–(e) 1.8*D* patterned cylinder ($\lambda_z/D = 1.8$) in the normal, interface, and fully coated part, respectively, at $U_r = 8.4$ where (i) to (iii) correspond to the location of the oscillating cylinder at $y^* = -y_0$, 0, and y_0.

(2) The superhydrophobic nature of the fully coated cylinder delays the onset of vortex shedding, resulting in a shift of the oscillation response to higher reduced velocities compared to the normal cylinder. In the initial branch, this coating effectively suppresses the VIV of the cylinder and reduces its hydrodynamic forces, albeit with slightly larger values observed in the lower branch. The maximum VIV amplitude and Cl_{rms} (root-mean-square lift coefficient) of the fully coated cylinder can be decreased by approximately 38.9% and 11.2%, respectively.

(3) The VIV amplitude versus reduced velocity (U_r) curve for the patterned cylinder exhibits a significant shift toward lower U_r values. Consequently, in the initial branch, the patterned cylinder experiences an increase of approximately 22.5% and 10.7% in the maximum VIV amplitude and Cl_{rms}, respectively.

Conversely, in the lower branch, the maximum VIV amplitude and Cl_{rms} of the patterned cylinder decrease by approximately 65.7% and 20.3%, respectively. These changes can be attributed to the three-dimensional flow structures revealed in the phase-averaged data analyses.

This research highlights the effectiveness of patterned superhydrophobic surfaces in VIV suppression, revealing their potential in real-world applications, such as marine structures, underwater cables, and related areas. However, owing to the equipment constraints, only two-dimensional PIV measurements are conducted on selected cylinders. More work will be done to explore the three-dimensional wakes and the dynamic response of various patterned cylinders in the future.

See the supplementary material for details the video intends to visually present and compare the flow dynamics of water passing over both the superhydrophobic and normal surfaces of the 1.8*D* patterned cylinder.

This study was financially supported by Natural Science Foundation of Guangdong Province (Project No. 2021A1515010337) and National Natural Science Foundation of China (Project No. 91952107).

AUTHOR DECLARATIONS

Conflict of Interest

The authors have no conflicts to disclose.

Author Contributions

Fuwang Zhao and Lingwei Zeng equally contributed to this work.

Fuwang Zhao: Conceptualization (equal); Data curation (equal); Funding acquisition (equal); Methodology (equal); Software (equal); Writing – original draft (equal); Writing – review & editing (equal). **Lingwei Zeng:** Data curation (equal); Formal analysis (equal); Methodology (equal); Software (equal); Writing – original draft (equal); Writing – review & editing (equal). **Zhaokun Wang:** Software (equal); Writing – original draft (equal); Writing – review & editing (equal). **Yang Liu:** Supervision (equal); Writing – original draft (equal); Writing – review & editing (equal). **Li Li:** Supervision (equal); Writing – original draft (equal); Writing – review & editing (equal). **Hui Tang:** Conceptualization (equal); Funding acquisition (equal); Investigation (equal); Supervision (equal); Writing – original draft (equal); Writing – review & editing (equal).

DATA AVAILABILITY

The data that support the findings of this study are available from the corresponding author upon reasonable request.

REFERENCES

[1]G. Hu, K. T. Tse, and K. C. S. Kwok, "Enhanced performance of wind energy harvester by aerodynamic treatment of a square prism," Appl. Phys. Lett. **109**(19), 193902 (2016).
[2]C. Wang, H. Tang, F. Duan *et al.*, "Control of wakes and vortex-induced vibrations of a single circular cylinder using synthetic jets," J. Fluids Struct. **60**, 160–179 (2016).
[3]H. Wang, L. Zeng, M. M. Alam *et al.*, "Large eddy simulation of the flow around a finite-length square cylinder with free-end slot suction," Wind Struct. **30**, 533–546 (2020).
[4]H. Wang, C. Zhao, L. Zeng *et al.*, "Control of the flow around a finite square cylinder with a flexible plate attached at the free end," Phys. Fluids **34**(2), 27109 (2022).
[5]L. Zeng, F. Zhao, H. Wang *et al.*, "A bi-directional flow-energy harvester," Appl. Phys. Lett. **122**, 153901 (2023).
[6]L. Zeng, F. Zhao, H. Wang *et al.*, "Control of flow-induced vibration of a circular cylinder using a splitter plate," Phys. Fluids **35**, 087104 (2023).
[7]F. Zhao, Z. Wang, H. Bai *et al.*, "Energy harvesting based on flow-induced vibration of a wavy cylinder coupled with tuned mass damper," Energy **282**, 128584 (2023).
[8]W. Wang and F. Zhao, "Numerical investigation on flow-induced vibration response of the cylinder inspired by the honeycomb," Ocean Eng. **268**, 113461 (2023).
[9]H. Choi, W. P. Jeon, and J. Kim, "Control of flow over a bluff body," Annu. Rev. Fluid Mech. **40**, 113–139 (2008).
[10]S. Rashidi, M. Hayatdavoodi, and J. A. Esfahani, "Vortex shedding suppression and wake control: A review," Ocean Eng. **126**, 57–80 (2016).
[11]W. Chen, Y. Huang, C. Chen *et al.*, "Review of active control of circular cylinder flow," Ocean Eng. **258**, 111840 (2022).
[12]M. Zhao, "A review of recent studies on the control of vortex-induced vibration of circular cylinders," Ocean Eng. **285**, 115389 (2023).
[13]Y. Ran, Z. Deng, H. Yu *et al.*, "Review of passive control of flow past a circular cylinder," J. Vis. **26**(1), 1–44 (2023).
[14]D. Quere and M. Reyssat, "Non-adhesive lotus and other hydrophobic materials," Philos. Trans. R. Soc., A **366**(1870), 1539–1556 (2008).
[15]D. You and P. Moin, "Effects of hydrophobic surfaces on the drag and lift of a circular cylinder," Phys. Fluids **19**(8), 81701 (2007).
[16]D. Legendre, E. Lauga, and J. Magnaudet, "Influence of slip on the dynamics of two-dimensional wakes," J. Fluid Mech. **633**, 437–447 (2009).
[17]G. McHale, N. J. Shirtcliffe, C. R. Evans *et al.*, "Terminal velocity and drag reduction measurements on superhydrophobic spheres," Appl. Phys. Lett. **94**(6), 64104 (2009).
[18]P. Muralidhar, N. Ferrer, R. Daniello *et al.*, "Influence of slip on the flow past superhydrophobic circular cylinders," J. Fluid Mech. **680**, 459–476 (2011).
[19]R. Daniello, P. Muralidhar, N. Carron *et al.*, "Influence of slip on vortex-induced motion of a superhydrophobic cylinder," J. Fluids Struct. **42**, 358–368 (2013).
[20]A. Rastegari and R. Akhavan, "On the mechanism of turbulent dragreduction with super-hydrophobic surfaces," J. Fluid Mech. **773**, R4 (2015).
[21]N. Kim, H. Kim, and H. Park, "An experimental study on the effects of rough hydrophobic surfaces on the flow around a circular cylinder," Phys. Fluids **27**(8), 85113 (2015).
[22]P. Sooraj, S. Jain, and A. Agrawal, "Flow over hydrofoils with varying hydrophobicity," Exp. Therm. Fluid Sci. **102**, 479–492 (2019).
[23]W. Choi, H. Byeon, J. Y. Park *et al.*, "Effects of pressure gradient on stability and drag reduction of superhydrophobic surfaces," Appl. Phys. Lett. **114**(10), 101603 (2019).
[24]P. Sooraj, M. S. Ramagya, M. H. Khan *et al.*, "Effect of superhydrophobicity on the flow past a circular cylinder in various flow regimes," J. Fluid Mech. **897**, A21 (2020).
[25]P. Bourrianne, C. Lv, and D. Quéré, "The cold Leidenfrost regime," Sci. Adv. **5**(6), eaaw304 (2019).
[26]J. D. Holmes, *Wind Loading of Structures* (CRC Press, 2018).
[27]K. Lei, Z. Tang, and Z. Sun, "Harvesting airflow energy from circular cylinder wake via a thin polyvinylidene fluoride film," J. Wind Eng. Ind. Aerodyn. **231**, 105235 (2022).
[28]K. Lei and Z. Sun, "A semicircular wall for harvesting wind energy from vortex-induced vibration and galloping," Ocean Eng. **280**, 114896 (2023).
[29]C. C. Feng, "The measurement of vortex induced effects in flow past stationary and oscillating circular and D-section cylinders," M.Sc. thesis (University of British Columbia, 1968).
[30]T. Zhou, S. F. M. Razali, Z. Hao *et al.*, "On the study of vortex-induced vibration of a cylinder with helical strakes," J. Fluids Struct. **27**(7), 903–917 (2011).

[31]G. R. S. Assi and P. W. Bearman, "Transverse galloping of circular cylinders fitted with solid and slotted splitter plates," J. Fluids Struct. **54**, 263–280 (2015).
[32]S. Liang, J. Wang, and Z. Hu, "VIV and galloping response of a circular cylinder with rigid detached splitter plates," Ocean Eng. **162**, 176–186 (2018).
[33]A. Khalak and C. H. K. Williamson, "Motions, forces and mode transitions in vortex-induced vibrations at low mass-damping," J. Fluids Struct. **13**(7–8), 813–851 (1999).
[34]P. W. Bearman, "Vortex shedding from oscillating Bluff bodies," Annu. Rev. Fluid Mech. **16**(1), 195–222 (1984).
[35]C. Wang, H. Tang, S. C. M. Yu *et al.*, "Control of vortex-induced vibration using a pair of synthetic jets: Influence of active lock-on," Phys. Fluids **29**, 83602 (2017).
[36]C. H. K. Williamson and R. Govardhan, "Vortex-induced vibrations," Annu. Rev. Fluid Mech. **36**, 413–455 (2004).